

# Laser annealing of Al implanted silicon carbide: Structural and optical characterization

C. Boutopoulos<sup>a</sup>, P. Terzis<sup>a,b</sup>, I. Zergioti<sup>a,\*</sup>, A.G. Kontos<sup>a</sup>, K. Zekentes<sup>b</sup>,  
K. Giannakopoulos<sup>c</sup>, Y.S. Raptis<sup>a</sup>

<sup>a</sup>National Technical University of Athens (NTUA), Physics Department, Iroon Polytehneiou 9, 15780 Zografou, Athens, Greece

<sup>b</sup>IESL, Foundation for Research and Technology-Hellas, Vassilika Vouton, PO Box 1527, 71110 Heraklion, Crete, Greece

<sup>c</sup>Institute of Materials Science, National Center for Scientific Research “Demokritos”, 15310 Ag. Paraskevi, Athens, Greece

Available online 24 February 2007

## Abstract

Pulsed-laser-based methods have been applied for post-implant annealing of p-type Al-doped 4H-SiC wafers in order to restore the crystal structure and to electrically activate the doping species. The annealing was performed with the third harmonic (355 nm) of a Nd:YAG laser at 4 ns pulse duration. The epilayers were characterized by micro-Raman spectroscopy under surface and cross-sectional backscattering. Changes in the phonon mode-intensity were related to the laser annealing induced recrystallization of the implanted material. The results were compared with changes in the infrared reflectivity across the Reststrahlen band. Transmission electron microscopy analysis showed the formation of columnar polycrystalline structure after the laser annealing process.

© 2007 Elsevier B.V. All rights reserved.

**Keywords:** Nd:YAG laser; Al-doped 4H-SiC surface; XeCl excimer laser; Electronic and optoelectronic devices; UV laser irradiation

## 1. Introduction

Silicon carbide (SiC) is a wide-band gap semiconductor with growing interest for the fabrication of electronic and optoelectronic devices. It has remarkable physical properties such as high electron mobility, high thermal conductivity and high breakdown field. Due to its special properties, SiC is suitable for high frequency, high temperature and high power devices [1]. Ion implantation has a crucial role in modern device fabrication since it offers controllability and reproducibility in planar doping semiconductors. The ion implantation of SiC causes crystal damage which in high doses leads to the formation of an amorphous surface layer [2,3]. In order to recover the crystal damage and activate the dopants, a high temperature annealing step over 1500 °C is required. The conventional method of furnace annealing at such a high temperature presents several disadvantages such as the redistribution of implanted dopants and surface roughness.

The use of pulsed laser allows the accumulation of energy in very short time into the near surface region while it maintains a low substrate temperature. Therefore, the laser annealing may be an alternative method for crystal damage recovering and electrically activating the dopants into SiC. Chou et al. [4] first demonstrated the removal of Ga implantation damage in 6H-SiC using a XeCl excimer laser and they found that molten SiC regrows epitaxially on the underlying substrate. They also reported significant redistribution of the implanted Ga. Ahmed et al. [5] have also used a XeCl excimer laser to electrically activate dopants into 6H-SiC. They measured complete activation of both n- and p-type dopants at a depth of 75 nm. Most of the groups used UV laser irradiation for their laser annealing experiments [4–8]. However, Camassel et al. [9] have recently reported the possibility of reducing the crystal damage using visible light laser irradiation at 532 nm. Raman and FTIR analysis showed that partial crystal recovery was achieved and they suggested the combination of conventional thermal with laser annealing processes. The ion implantation increases dramatically the absorption coefficients of the implanted layers in the range between 200 and 800 nm in comparison to the pure crystalline SiC [10]. An efficient

\* Corresponding author. Tel.: +30 210 7723345; fax: +30 210 7723338.

E-mail address: [zergioti@central.ntua.gr](mailto:zergioti@central.ntua.gr) (I. Zergioti).

method to irradiate the sample at a high energy density and to avoid surface damage has first been reported by Tanaka et al. [8] as “multiple energy irradiation method”. It is based on a subsequent irradiation with steps of increased energy density. The lowest energy fluence anneals the upper ion implanted layers and as the energy fluence is increased, deeper layers may be annealed without ablation and damage.

In our previous work [11] we have presented some preliminary studies of 355 nm and 532 nm laser annealing of Al-doped 4H-SiC, where we had the first indication that the use of 355 nm was more efficient for the crystal recovery of the Al-doped 4H-SiC surface. The use of the 355 nm gives a higher optical absorption because the energy of the photons is close to band gap of the 4H-SiC which is 3.23 eV.

The aim of this work is to investigate the effect of the laser irradiation on the structural and optical properties of an Al implanted 4H-SiC sample, in relation to the laser annealing parameters using the third harmonic (355 nm) of a Nd:YAG laser. Surface and cross-sectional Raman spectroscopy were used to investigate the crystal quality of the as-implanted and the laser annealed SiC. This method has widely used for SiC characterization since it is non-destructive, requires no special sample preparation and presents high sensitivity on structural changes [12–14]. The samples were also analyzed by TEM and reflectance Fourier transform infrared spectroscopy (FTIR), which is a powerful tool for investigating the ion implantation induced SiC crystal damage [15,16] and its repair by laser irradiation [17].

## 2. Experimental

Experimental investigations were made on a commercially available 4H-SiC sample purchased by Cree Research Inc. The epitaxial structure consist of two layers and it was grown on  $n^+$ -type (resistivity: 0.018  $\Omega$  cm), 2 inch in diameter, 4H-SiC substrate 8° off with a thickness of 417  $\mu$ m. On top, a “field-stop” layer of 0.5  $\mu$ m thick with n-type doping of  $1 \times 10^{18}$   $\text{cm}^{-3}$  was deposited. The second epilayer has a thickness of 10  $\mu$ m and n-type doping of  $6.8 \times 10^{15}$   $\text{cm}^{-3}$ . In order to achieve a flat p-type dopant profile, multiple energy Al ion implantation was performed. More precisely, the implant energies were 25, 60, 115, 195 and 300 keV while the Al doses were  $0.24 \times 10^{14}$ ,  $0.50 \times 10^{14}$ ,  $0.73 \times 10^{14}$ ,  $1.0 \times 10^{14}$  and  $2.1 \times 10^{14}$   $\text{cm}^{-2}$ , respectively. A mean concentration of  $10^{19}$  Al/ $\text{cm}^{-3}$  over approximately 0.5  $\mu$ m was targeted with a total dose of  $4.57 \times 10^{14}$   $\text{cm}^{-2}$ .

The irradiation of the sample was carried out using the third harmonic (355 nm) of a Nd:YAG laser. Several optical components were used to control the laser fluence and to ensure a uniform distribution of the laser beam on the sample. The energy density varied between 0.15 and 0.75 J/ $\text{cm}^2$ , while the number of pulses ranged from 100 to 1000. Furthermore, we have applied the ‘multiple irradiation method’ by increasing gradually the laser fluence on the same spot. More specifically, we have performed consequent irradiations, under the energy-densities of 0.15, 0.25 and 0.35 J/ $\text{cm}^2$ , with the same number of pulses for each density. The whole procedure has been repeated

for two different total number of pulses ( $3 \times 33 = 99$  and  $3 \times 100 = 300$  pulses).

The irradiated areas were morphologically examined by optical microscopy and scanning electron microscopy (SEM). Room temperature infrared reflectance measurements were carried out at near normal incidence (13°) using a Bruker IFS 66v/S Fourier transform infrared spectrometer (FTIR). Each sample received 32 scans at a resolution of 1  $\text{cm}^{-1}$  between 400 and 7800  $\text{cm}^{-1}$ . An aluminum mirror was used as the reference reflector and the change in reflectivity was measured to be <0.5% across the complete spectral range after 1 h operation. Surface and cross-sectional micro-Raman spectroscopy was performed using a triple Jobin-Yvon spectrometer operating in the subtractive mode and equipped with a CCD detector. Spectra were recorded after focusing the 488 nm line of an Ar<sup>+</sup> laser on a 1  $\mu$ m spot of the sample, under 1–2 mW power. Cross-sectional TEM studies were carried out with a Philips CM 20 transmission electron microscope operating at 200 keV equipped with an energy dispersive X-ray spectrometer and an electron energy loss spectrometer.

## 3. Results and discussion

The surface analysis by SEM, of the irradiated areas showed that the surface roughness was not changed when the laser density was below 0.35 J/ $\text{cm}^2$ . In reverse, the surface roughness was increased by irradiation at energy densities above 0.35 J/ $\text{cm}^2$ , indicating that the material had melted. At 0.75 J/ $\text{cm}^2$ , we observed that the surface was ablated.

In Fig. 1, different IR reflectance spectra collected for the as-implanted, the as-grown and the laser annealed samples using 355 nm laser pulses are depicted. Ion implantation has caused the decrease of the reflectivity of the Reststrahlen band (770–970  $\text{cm}^{-1}$ ) in comparison to the spectrum collected from the non-implanted sample. By irradiating at 0.15 J/ $\text{cm}^2$ , a small increase of the Reststrahlen-band intensity was observed. The annealed sample with the ‘multiple irradiation method’ (0.15–0.25–0.35 J/ $\text{cm}^2$ , 33 or 100 pulses) has the maximum reflectivity, indicating that irradiation with the ‘multiple irradiation method’ was the most effective to anneal the crystal damage. It is mentioned that the interference pattern, appeared in the spectral region above 1000  $\text{cm}^{-1}$ , is related to the existence of different layers in our sample. The peak which appears at about 1050  $\text{cm}^{-1}$  is an artificial spike present in all spectra.

As-implanted and laser-annealed, 4H-polytype SiC samples, have been studied by means of micro-Raman characterization techniques. The measured spectra are mainly analyzed in terms of the transverse optical (TO)  $E_{2T}$  (776  $\text{cm}^{-1}$ ),  $A_{1T}$  (783  $\text{cm}^{-1}$ ), and  $E_{1T}$  (798  $\text{cm}^{-1}$ ) Raman bands, which are shown in the literature [18] to be not affected by carrier effects, (in contrary the axial- $A_{1L}$  (964.5  $\text{cm}^{-1}$ ) and the planar- $E_{1L}$  (966.8  $\text{cm}^{-1}$ ) modes are broadened and shifted to the higher frequency side, in the case of the n-type samples [12,18]). The two separate subgroups of the Raman bands, TO modes  $E_{2T}$ ,  $A_{1T}$  and  $E_{1T}$  on the one hand, and  $A_{1L}$  and  $E_{1L}$ , on the other, could be used, in a complementary way, to characterize the lattice and the carrier

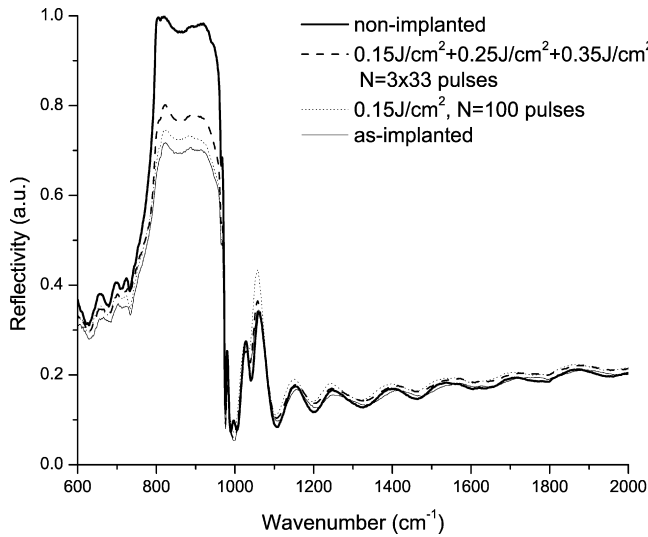


Fig. 1. Infrared reflectivity spectra of non-implanted, as-implanted and laser annealed 4H-SiC samples at 355 nm.

properties, respectively, of the near-surface thin layer, provided that they could be simultaneously monitored in a spectroscopic measurement. The “face” and “side” backscattering measurements, accessible through micro-Raman techniques, are offering such a possibility, as it will be shown below.

Cross-sectional micro-Raman measurements have been performed. A logarithmic vertical scale is used in order to present both high and low intensity details. The results of these side-measurements are summarized in Fig. 2. Fig. 2(a) presents a micro-Raman spectrum measured from the heavily doped ( $n^+$ ) 4H-SiC substrate, with characteristic peaks at  $610\text{ cm}^{-1}$  (folded longitudinal acoustic mode—FLA of 4H-SiC [18]),  $783.9$ ,  $798.8$  and  $839.8\text{ cm}^{-1}$  (folded longitudinal optical mode—FLO of 4H-SiC [18]). The broad asymmetric band, peaked at  $984\text{ cm}^{-1}$ , is the coupled mode (CPLP: coupled plasmon-longitudinal-phonon) between the collective plasma excitation (plasmon), due to the high concentration of the  $n$ -type free carriers, and the LO-phonon ( $E_{IL}$ ,  $967\text{ cm}^{-1}$ , as it can be confirmed by the next spectra c–e). In Fig. 2(b), moving to a less doped area, we have a decrease of the CPLP mode contribution together with a shift toward the lower frequencies. The next three spectra (c–e) come from the top Al-implanted  $p$ -type layer. Since the excitation spot has a diameter of ( $\approx 1\text{ }\mu\text{m}$ ), which is greater than the thickness of the top implanted layer ( $\approx 0.5\text{ }\mu\text{m}$ ), the measurement has been taken with half of the excitation spot out of the sample, in order to minimize the unwanted contribution from the  $n$ -type region. As it is evident from Fig. 2(c)–(e), the high frequency contribution is diminished, while a weaker activity appears in the low-frequency side of the  $967\text{ cm}^{-1}$  peak. This feature is probably due to the  $p$ -type carriers of the Al-implanted layer and their interaction with the longitudinal mode. This activity shows a slightly different shape, between (c) and (d and e), close to the base of the sharp peak ( $969\text{ cm}^{-1}$ ), which might be an indication of the annealing-influence on the top-layer Al-implants. In addition, the broad feature centered around  $540\text{ cm}^{-1}$ , appears in the spectra of the top layer while it is

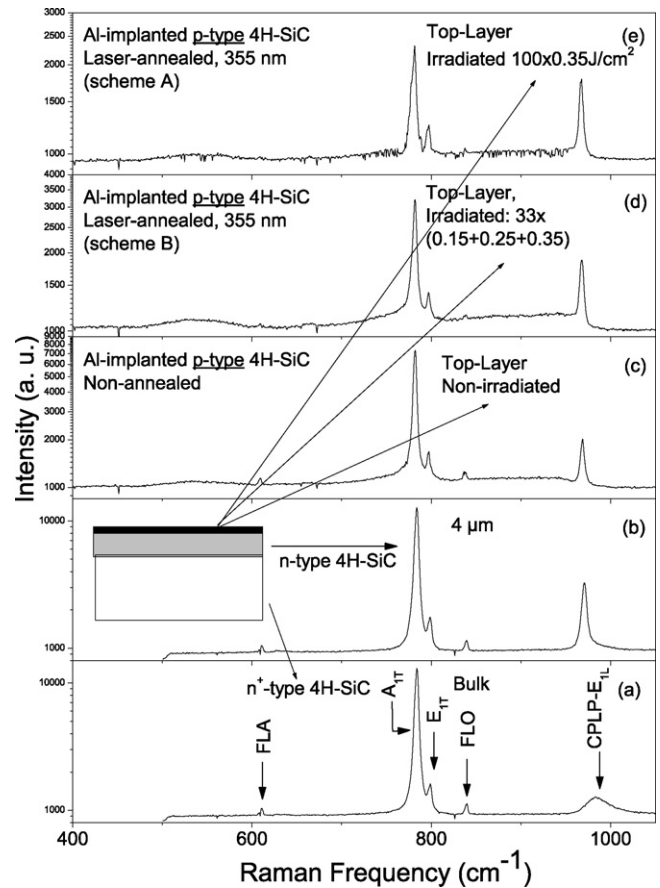


Fig. 2. Cross-sectional micro-Raman backscattering spectra from different regions of the as-implanted sample as well as the top layer of various irradiated samples.

missing from the deeper region. This feature, therefore, seems not to be related to the electronic Raman scattering from nitrogen defect levels, under IR excitation, as it is reported in the literature [19] and is probably related to Al.

However, we could not confirm the electrical activation by electrical measurements due to difficulties in achieving ohmic contacts.

The side-view measurement has been combined with a front-view micro-Raman backscattering of the as-implanted and the laser-annealed areas, under different annealing schemes. The results of this investigation are summarized in Fig. 3. With the exception of the irradiation with 100 pulses, at  $0.75\text{ J/cm}^2$ , the spectra from the as-implanted and all the other laser-annealed regions, exhibit the same qualitative characteristics, which have been already analyzed in the previous paragraph, by means of the cross-section measurements. The spectrum from the region annealed with 100 pulses, at  $0.75\text{ J/cm}^2$ , presents a diminishing scattering from the SiC crystalline phase as well as a broad band of the amorphous Si (a-Si) centered at around  $480\text{ cm}^{-1}$ , and a sharp peak of the crystalline Si (c-Si) at  $520\text{ cm}^{-1}$ . Apparently dissociation of SiC combined with the formation of amorphous and crystalline Si is caused by the high laser fluence.

From the regions annealed under lower energy-densities, in spite of the qualitative similarities of the spectra, we can monitor a quantitative systematic change, regarding the

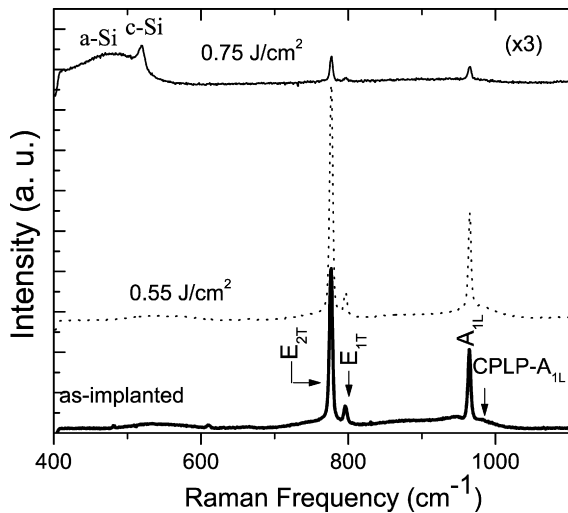


Fig. 3. Characteristic front-view backscattering micro-Raman spectra of as-implanted and laser-annealed samples. Spectra are shifted for clarity.

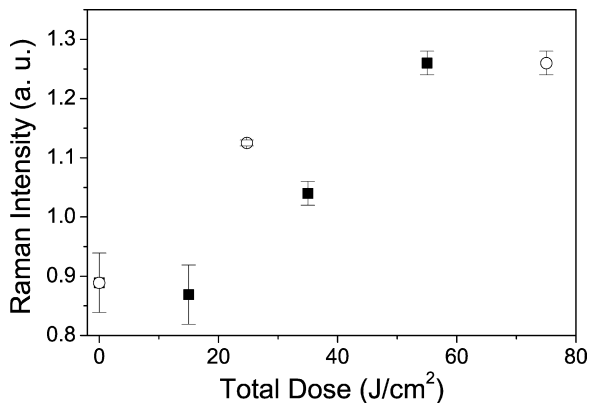


Fig. 4. The integrated intensity of the transverse optical  $E_{2T}$  ( $776\text{ cm}^{-1}$ ) mode, as a function of the total energy dose of the annealing laser beam at  $355\text{ nm}$ , for (a) a sequence of samples irradiated with 100 pulses and energy density per pulse,  $0.15$ ,  $0.35$  and  $0.55\text{ J/cm}^2$  (solid squares) and (b) a sequence of samples treated by the ‘multiple irradiation method’ at  $0.15$ ,  $0.25$  and  $0.35\text{ J/cm}^2$  with either 33 or 100 pulses at each energy (open circles).

absolute scattering intensity, which is attributed to the recrystallization of the Al implanted layer [14]. A display of the above observations is presented in Fig. 4, where the integrated intensity of the (TO)  $E_{2T}$  ( $776\text{ cm}^{-1}$ ) mode of the

crystalline SiC, is shown as a function of the total energy dose of the annealing laser beam. Two sequences of conditions are presented, samples annealed at various energy densities and 100 pulses (solid squares) and samples treated by the ‘multiple irradiation method’ at  $0.15$ ,  $0.25$  and  $0.35\text{ J/cm}^2$  with either 33 or 100 pulses at each energy (open circles).

As it is evident from Fig. 4, taking the integrated intensity as a measure of the crystal-quality, by increasing the energy-density we have a better recovery of the crystallinity, which was reduced by the implantation procedure. As it is shown, the ‘multiple irradiation method’, seems to be more efficient, for the intermediate total energy doses. The integrated Raman intensity saturates with both methods (similar degree of recrystallization), although the multiple irradiation one requires a higher total dose. Nevertheless, as it can be visually observed through specular reflection from the sample, and confirmed by electron microscopy (SEM), a lower roughness of the annealed surface can be achieved, in the case of multiple irradiation. This indicates a much more effective interaction of the annealing-beam with the SiC surface, in the multiple irradiation case, which needs further investigation and analysis.

TEM analysis has shown the formation of columnar polycrystalline structure after the laser annealing process. Fig. 5(a) and (b) shows cross-sectional bright and dark field TEM images from a laser annealed sample under the ‘multiple irradiation conditions’, ( $0.15$ – $0.25$ – $0.35\text{ J/cm}^2$ ,  $3 \times 33$  pulses). Two zones are depicted, the zone I which is the recrystallized columnar structure and starts from the surface to a depth between  $240$  and  $280\text{ nm}$ . The zone II is the remaining damaged implanted layer which has thickness between  $100$  and  $140\text{ nm}$ . Similar results are reported by Hedler et al. [6] who found a recrystallised layer of  $200\text{ nm}$  and a remaining amorphous layer of  $150\text{ nm}$  after the KrF laser annealing process. In-Tae Bae et al. [20] have observed a complete epitaxial recrystallization of the cubic phase of SiC followed by thermal annealing at  $940\text{ }^\circ\text{C}$ . Moreover, the TEM results confirm the conclusions of Raman and FTIR analysis concerning the improved recrystallization through the ‘multiple irradiation method’.

#### 4. Conclusions

In conclusion, we have performed preliminary studies of laser annealing of Al-doped 4H-SiC using  $355\text{ nm}$ . The as-implanted and the laser-annealed 4H-SiC samples were

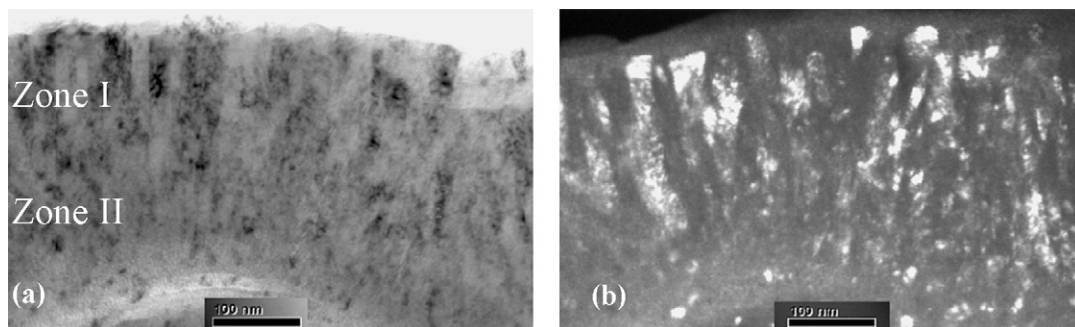


Fig. 5. (a) Bright field and (b) dark field cross-sectional TEM images of the laser annealed 4H-SiC/Al implanted under the multiple irradiation method.

examined by infra-red reflectivity measurements and micro-Raman spectroscopy under surface and cross-sectional back-scattering. The changes in the phonon mode intensity were related to the laser annealing induced recrystallization of the implanted 4H-SiC material. The Raman and the FTIR analysis showed that the ‘multiple irradiation method’ was more efficient for the crystal recovery of the Al-doped 4H-SiC surface. TEM analysis has revealed the recrystallized columnar structure after the laser annealing.

### Acknowledgments

The project is co-funded by the European Social Fund (75%) and National Resources (25%)—Operational Program for Educational and Vocational Training II (EPEAEK II) and particularly the Program PYTHAGORAS II. The authors would like to thank IBS, France for the implantation of the samples.

### References

- [1] P.G. Neudeck, in: K.H.J. Bushchow, R.W. Cahn, M.C. Flemings, B. Ilshner, E.J. Kramer, S. Mahajan (Eds.), *Encyclopedia of Materials: Science and Technology*, vol. 9, Elsevier Science, Oxford, 2001, p. 8508.
- [2] E. Wendler, A. Heft, W. Wesch, *Nucl. Inst. Methods B* 141 (1998) 105.
- [3] W.J. Weber, L.M. Wang, N. Yu, *Nucl. Inst. Methods B* 116 (1996) 322.
- [4] S.Y. Chou, Y. Chang, K.H. Weiner, T.W. Sigmon, *Appl. Phys. Lett.* 56 (6) (1990) 530.
- [5] S. Ahmed, C.J. Barbero, T.W. Sigmon, *Appl. Phys. Lett.* 66 (6) (1995) 712.
- [6] A. Hedler, S. Urban, F. Falk, H. Hobert, W. Wesch, *Appl. Surf. Sci.* 205 (2003) 240.
- [7] C. Dutto, E. Fogarassy, D. Mathiot, D. Muller, P. Kern, D. Ballutaud, *Appl. Surf. Sci.* 208–209 (2003) 292.
- [8] Y. Tanaka, H. Tanoue, K. Arai, *J. Appl. Phys.* 93 (10) (2003) 5934.
- [9] J. Camassel, H. Pyere, D.J. Brink, M. Zielinski, S. Blanque, N. Mestres, P. Godignon, *Mater. Sci. Forum* 457–460 (2004) 941.
- [10] G. Derst, C. Wilbertz, K.L. Bhatia, W. Kratschmer, S. Kalbitzer, *Appl. Phys. Lett.* 54 (18) (1989) 1722.
- [11] I. Zergioti, A.G. Kontos, K. Zekentes, C. Boutopoulos, P. Terzis, Y.S. Raptis, *SPIE International Conference on High Power Laser Ablation*, vol. 6261, 2006, p. 626135.
- [12] S. Nakashima, H. Harima, *Phys. Status Solidi (A)* 162 (1997) 39.
- [13] H. Hobert, H. Dunken, R. Menzel, T. Bachmann, W. Wesch, *J. Non-Cryst. Solids* 220 (1997) 187.
- [14] J. Camassel, S. Blanque, N. Mestres, P. Godignon, J. Pascual, *Phys. Status Solidi (A)* 195 (2003) 875.
- [15] H. Hobert, H. Dunken, F. Seiferta, R. Menzel, T. Bachmann, W. Wesch, *Nucl. Inst. Methods B* 129 (1997) 244.
- [16] A. Declémy, E. Oliviero, M.F. Beaufort, J.F. Barbot, M.L. David, C. Blanchard, Y. Tessier, E. Ntsoenzok, *Nucl. Inst. Methods B* 186 (2002) 318.
- [17] P.H. Key, D. Sands, M. Schlaf, C.D. Walton, C.J. Anthony, K.M. Brunson, M.J. Uren, *Thin Solid Films* 364 (2000) 200.
- [18] H. Harima, S. Nakashima, T. Uemura, *J. Appl. Phys.* 78 (3) (1997) 1996.
- [19] J.C. Burton, F.H. Long, I.T. Ferguson, *J. Appl. Phys.* 86 (4) (1999) 2073.
- [20] I.-T. Bae, M. Ishimaru, Y. Hirotsu, *Jpn. J. Appl. Phys.* 44 (8) (2005) 6196.